PCCP

Accepted Manuscript

ROYAL SOCIETY OF CHEMISTRY

www.rsc.org/pccp

GRAPHICAL ABSTRACT

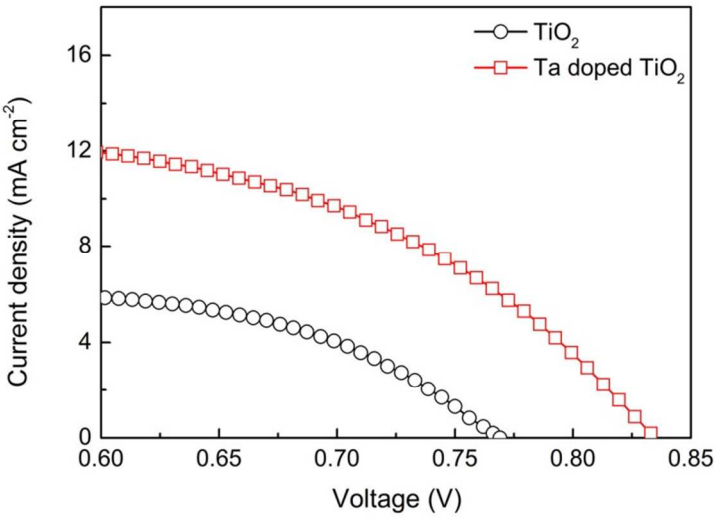

Enhanced electron concentration is responsible for the open-circuit voltage improvement due to the upward shift of the Fermi level.

Cite this: DOI: 10.1039/c0xx00000x

www.rsc.org/xxxxxx

ARTICLE TYPE

Open-Circuit Voltage Improvement from Tantalum Doped TiO_2 Nanocrystals

Feng Gu,*[ab] Wenjuan Huang,[a] Shufen Wang,[a] Xing Cheng,[a] Yanjie Hu,*[a] Pooi See Lee[b]

Received (in XXX, XXX) Xth XXXXXXXXX 20XX, Accepted Xth XXXXXXXXX 20XX

DOI: 10.1039/b000000x

Enhanced electron concentration derived from Ta^{5+} doping is responsible for the open-circuit voltage improvement due to the upward shift of the Fermi level, but the oxygen defects generated retards the negative shift of Fermi level. By mediating the trap states, highly efficient DSSC devices could be achieved.

Dye-sensitized solar cells (DSSCs) have been widely studied as a promising new type of photovoltaic devices because of their easy fabrication, low cost, and flexibility, compared with the conventional, rigid silicon wafer-based technologies[1] Apart from the current research hot topic on further increasing DSSC efficiency by developing alternate electrode materials offering longer electron diffusion lengths,[2-4] the development of DSSC devices with high open-circuit photovoltage (V_{oc}) has attracted increasingly great attention as the improvement of V_{oc} would extend the applicability of DSSCs.[5, 6] Generally, the V_{oc} of a liquid-junction DSSC is determined by the energy difference between the quasi-Fermi level of the semiconductor and the potential of the redox couple in the electrolyte.[7] For TiO_2-based DSSCs, theoretical maximum achievable value of V_{oc} is estimated to be 0.95V.[6] However, V_{oc} values of only 0.7-0.8V have been yielded for the current DSSC devices due to the high interfacial recombination losses.[8] Heterostructures and conformal barrier layers are always engineered in the TiO_2-based photoelectrode film to minimize the interfacial charge recombination losses and only approximate 50mV improvement in the open-circuit photovoltage could be yielded.[9, 10]

Recently, impurity doping has been emerging as one feasible strategy to improve device performance by tailing the band gap structure and electric conductivity of semiconductor oxides.[11, 12] Remarkable improvement in efficiency has been achieved by suitably doping ions such as Nb, Al, N, Cr, W and Cu into TiO_2 electrode film mainly to promote electron injection by creating trap states in the gap.[13, 14] Although remarkable increment in V_{oc} has been achieved,[15, 16] the mechanism and effect of doping states on the V_{oc} variability are still unclear. Now it is well established that the V_{oc} increment is closely correlated to the movement of the flat band potential and the Fermi level.[6] But the trap sites created by conventional doping ions made the band edge to positively shift and the Fermi level is affected by the defects simultaneously.[17, 18] Previous works even demonstrated opposite contribution to the V_{oc} by doping with same ions. For example, a very high V_{oc} of 0.87V from Ta-doped rutile TiO_2 nanowire arrays prepared by hydrothermal method have been reported recently.[6] However, a totally different result was presented for Ta-doped TiO_2 nanotube layers by anodization of Ti-Ta alloys and Ta-doped TiO_2 inverse opals by atomic layer deposition (ALD) method with showing decreased V_{oc} upon Ta doping.[19, 20] Therefore, it is necessary to study the possibilities of doping states as the mechanism to improve the V_{oc} when we explore highly efficient DSSCs, especially with higher V_{oc} for special applications.

Herein, Ta ions were first introduced into TiO_2 host by using an efficient flame spray pyrolysis (FSP) approach. The FSP approach possesses an inherent advantage for preparing high-quality nanoparticles with unique morphology, but it is challenging to dope impurity ions homogeneously in the flame because of the disparate rates of hydrolysis/oxidation of the volatile metal chlorides. In this work, we used FSP approach by employing combustible, high enthalpy-content organic solution (alcohol solution of organometallic) with dissolving doping ions as precursor, which was aerosolized with oxygen and ignited in the flame. Homogeneous Ta doping could be achieved in such short flame reaction duration and homogeneous doping of other metal cations could also be expected by this fast doping process for potential applications in photoelectric conversion and catalysis. By mediating the trap states in the host, the V_{oc} was increased greatly (~9%) under optimal doping condition for liquid-state DSSCs and highly efficient DSSC devices could also be achieved due to the enhanced charge injection.

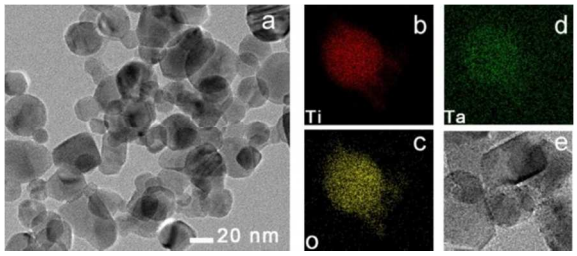

Fig. 1 TEM images of Ta-doped TiO_2 nanoparticles (a, e). Element mapping images of one doped particle (b-d).

The formation of doped TiO_2 nanoparticles followed the typical liquid-feed FSP process.[21, 22] The alcohol solution of titanium tetrabutoxide and trace amount $TaCl_5$ was aerosolized by oxygen and then ignited. Homogeneously doped TiO_2 nanoparticles would be formed after precursor conversion by nucleation from the gas phase and grow by surface reaction

and/or coagulation and subsequent coalescence into larger particles. Fig. S1 shows X-ray diffraction (XRD) patterns of the undoped and Ta-doped TiO_2 with different Ta contents. The diffraction peaks sharpened after Ta doping, implying better crystallinity. All peaks of the undoped sample can be assigned to the anatase phase. Ta doping could induce the anatase to rutile phase tranformation with the presence of (110) diffraction peaks of rutile TiO_2 and the diffraction peaks shift to lower angles with increasing Ta content (inset of Fig. S1), indicating the host lattice deforms with lengthening Ti-O bonds after Ta substitution of Ti at the octahedral sites. The content of the rutile phase in the products are estimated to be 1.2%, 2.5%, 3.4% and 5.7%, respectively, when the doping concentration varies from 0.1 to 0.4% (Fig. S1b). Typical transmission electron microscopy (TEM) image shown in Fig. 1a reveals that the Ta-doped TiO_2 nanoparticles are highly crystalline and the average size is about 30 nm. Scanning electron microscopy (SEM) and TEM images of the pristine TiO_2 nanoparticles are shown in Fig. S2. To distinguish the distribution of Ta in the particle, energy-filtered imaging was performed. Energy-dispersive X-ray spectrometry (EDS) mapping analyses of elements Ti, Ta, and O (Fig. 1b-d) from a single particle confirmed the Ta doping is very homogeneous. It is noted that, strong signals from Ta and O can still be detected around TiO_2 nanoparticle, whereas the secondary phase could not be detected from XRD measurements. This phenomenon suggests only partial Ta has been introduced into TiO_2 nanocrystal during the flame reaction. The actual doping concentration was estimated by measuring X-ray photoelectron spectroscopy (XPS) and the results are shown in Table S1. From these results, we can find that about half Ta ions could be doped into the TiO_2 host. An ion substituting Ti^{4+} in the crystalline lattice may either hinder or anticipate the transformation depending on whether oxygen vacancy concentration is decreased or increased.[23] Impurities like Ta^{5+} and Nb^{5+} could reduce the number of oxygen vacancy, thus the phase transition was retarded. However, in our work, rutile TiO_2 appeared after Ta doping and the rutile content was increased with doping concentration. It is noted that during the fast FSP process, partial Ta ions, especially those at the interstitial positions, would get enough energy from the high temperature of flame reaction and would be expelled from the anatase structure with the presence of oxygen vacancies act as nucleation sites,[23] consequently, a fast transformation to rutile may occur. The formation of rutile TiO_2 would be constructive to the separation of photoexcited charge carriers and decrease the recombination rates.[24] After being segregated from the antanse TiO_2, the Ta aggregates are likely to present in the form of TaO_x in the H_2/air flame field (Fig. 1e).

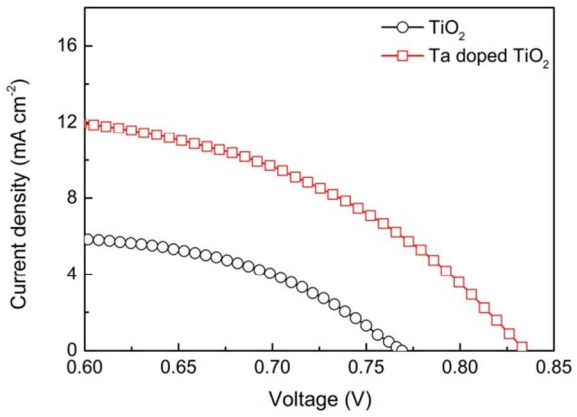

Fig. 2 J-V curves of the DSSC devices using the pristine TiO_2 and 0.3% Ta-doped TiO_2 (with$TiCl_4$ treatment).

Table 1 Performance characteristics of the DSSCs.

Cell[a]	V_{oc} (V)	J_{sc} (mA cm^{-2})	FF	η(%)
TiO_2	0.769	5.552	70.832	3.154
0.1Ta-TiO_2	0.800	7.164	68.371	4.163
0.2Ta-TiO_2	0.808	8.702	68.035	4.839
0.3Ta-TiO_2	0.825	8.582	67.722	4.834
0.4Ta-TiO_2	0.817	7.064	70.352	4.075
0.1Ta-TiO_2*	0.809	12.389	67.645	6.777
0.2Ta-TiO_2*	0.815	14.158	65.165	7.502
0.3Ta-TiO_2*	0.835	13.079	66.431	7.245
0.4Ta-TiO_2*	0.829	12.549	64.633	6.721
0.2Ta-TiO_2*#	0.814	18.795	56.690	8.659

[a] The active areas of the photoelectrodes were 0.25 cm^2. [*] Electrode films with $TiCl_4$ treatment. [#] Electrode film under heat-treatment in Ar.

We experimentally examined the performance of the photoelectron-conversion efficiency of the Ta-doped TiO_2 photoanodes with different doping concentrations. The powders should be rinsed thoroughly before electrode fabrication to exclude the effect from the isolated tantalum species. The characteristic current (J) -voltage (V) curves of these DSSC devices are given in Fig. 2, and their photovoltaic parameters are summarized in Table 1. Under illumination of simulated sunlight (60mW cm^{-2}), the energy conversion efficiencies increase gradually from 3.154 to 4.839% when the doping concentration varies from 0 to 0.2% and then decreased to 4.075% when further increasing the doping concentration to 0.4%. It should be noted that the V_{oc} reached 0.825V when doping 0.3% Ta into the host, which is obviously higher than that of pristine TiO_2 (0.769V). Apart from V_{oc}, short-circuit current density (J_{sc}) of the doped electrode is superior to that of the pristine TiO_2 counterpart. The amount of dye absorption was increased a little after doping Ta into the host. For example, the amounts of dye absorption were 4.302×10^{-8} and 4.760×10^{-8} mol cm^{-2} for pristine and 0.2% Ta-doped TiO_2 electrodes. It has been reported that when the dye loading increases by 1.2 times, the incident-photon-to-current efficiency (IPCE) only increased approximately by 3%.[13, 25] Therefore, we can conclude that the intrinsic increases in the photocurrent are primarily due to the enhanced electron injection. Furthermore, after $TiCl_4$ treatment, the Ta-doped device yielded higher efficiencies and the V_{oc} was further increased to 0.835V for 0.3% Ta-doped TiO_2 electrode due to the enhanced electron injection arising from the increased dye loading capability. For 0.3% Ta-doped TiO_2 electrode, the amount of dye absorption was increased from 4.774×10^{-8} mol cm^{-2} to 9.352×10^{-8} mol cm^{-2} after $TiCl_4$ treatment.

It is known that the V_{oc} is closely related to the flat band potential and the Fermi level of semiconductor. Mott-Schottky and photocurrent density-potential analyses were employed to better understand the band energetics of the Ta-doped TiO_2 electrode. From the Mott-Schottky plots shown in Fig. 3a, it is clear that the flat band edge shows an obvious negative shift with Ta doping concentration, which elongates the difference with the potential of the redox couple in the electrolyte. Fig. 3b shows photocurrent density-potential curves of the Ta-doped and undoped samples. Clearly the open-circuit potential of the Ta-doped electrode is negatively shifted by ~200 mV compared with the undoped electrode. The negative shift can be attributed to the improved electron concentration and trap distribution caused by tantalum doping. The negative shift in the flat-band potential and open-circuit potential under illumination in Ta-doped samples suggests that the V_{oc} enhancement in the DSSCs is caused by a higher quasi-Fermi level in the doped electrode.

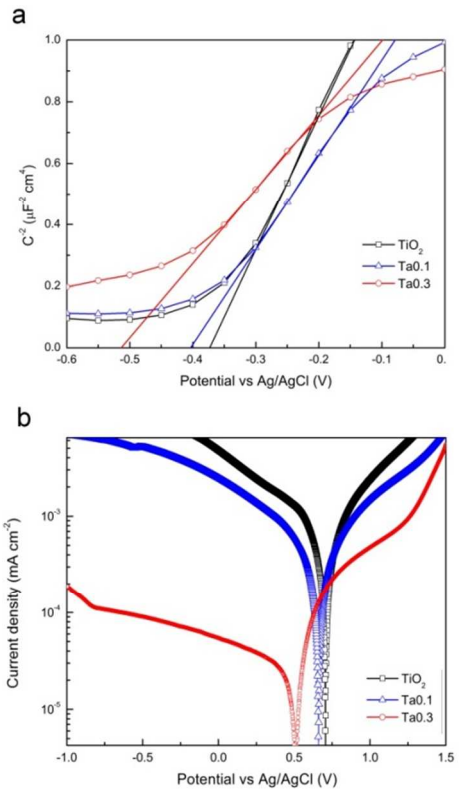

Fig. 3 Mott-Schottky plots (a) and photocurrent density-applied potential curves (b) of pristine TiO_2 and Ta-doped TiO_2 electrodes in KCl and Na_2SO_4 electrolyte solutions, respectively. (Ag/AgCl reference electrode).

As tantalum has a 5+ valence and an ionic radius similar to that of Ti^{4+}, thus the introduction of tantalum increases the electron concentration with the formation of Ti^{3+} in the host for charge compensation.[26] The electrons partially fill the surface traps, leading to an upward shift of the Fermi level, which leads to the larger V_{oc} for the DSSCs when using the Ta-doped TiO_2 nanoparticles. The electron concentration is predicted to increase rapidly with doping tantalum content. Ti^{3+} states in the host could be verified by XPS measurements (Fig. S3). With increasing the Ta concentration, the Ti^{4+} $2p_{3/2}$ peak at ~458 eV shifted slightly to lower binding energies, indicating a gradual increase of Ti^{3+} content.[27] However, excess Ta content would cause high defect concentration (e.g., oxygen vacancies formed after interstitial Ta migration) and the electron mobility would decrease rapidly due to the electron scattering by the defects.[13] To further study the Ti^{3+} content dependence on electron concentration, the doped sample was heat-treated at 450°C in Ar in order to prevent the oxidation to Ti^{3+}. The color of the sample powders varied from light blue to grey (Fig. S4). Ti^{4+} $2p_{3/2}$ peak also shifted to lower binding energies a little further, implying Ti^{3+} could be well preserved upon heat treatment in Ar. However, the V_{oc} of the fabricated electrode showed a slight decrease instead of increase, for example, 0.814V for the electrode doped with 0.2% Ta. But the efficiency of the device after inert atmosphere treatment was increased greatly up to 8.659%, almost 15% higher than that of the counterpart heat-treated in air. The prominent increment in efficiency can be attributed to the formation of color centers in the host after being heat-treated in Ar.[28] Under this non-oxygen heattreatment, the doped tantalum may migrate out from the substitution sites with the formation of oxygen vacancies in the host, which are known to form deep trap states ~0.7-0.8eV below the conduction band.[29] In TiO_2 and other metal oxides, the color centers associated with oxygen vacancies are the F, F^+, and F^{++} centers with different numbers of trapped electrons. The deep trap states derived from the advent of color centers are believed to enhance the electron injection remarkably and higher performance of the DSSCs device will be yielded.

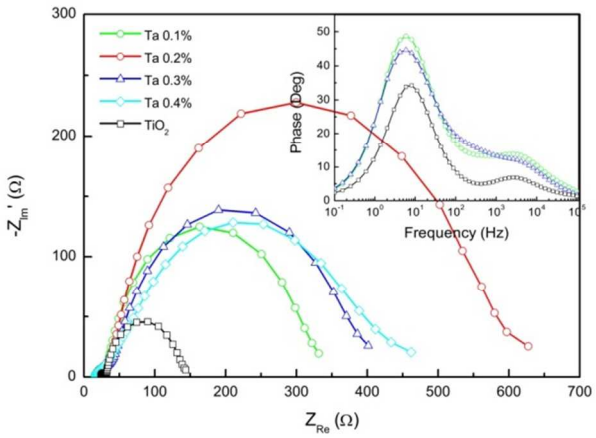

Fig. 4 EIS spectra and corresponding Bode-phase plots of fabricated DSSC devices using TiO_2, and Ta-doped TiO_2 electrodes.

Electrochemical impedance spectroscopy (EIS) was used to study the electron transfer in the doped electrode film as by which the internal resistances and charge transports at the interfaces in DSSCs can be analysed.[30] The semicircle in the frequency range of 100-1Hz is associated with the charge transfer across the photoanode/electrolyte interface. From the Nyquist plots of the impedance spectra shown in Fig. 4, it is obvious that the second semicircle becomes remarkably bigger after Ta doping, implying much slower electron recombination in the doped electrode, which is correlated with the improved electron concentration in the electrode and the negative shift of V_{fb} after doping. Excess Ta doping would cause the formation of deep trap states inevitably, which would promote charge recombination at photoanode/electrolyte interface, consequently, the semicircle became smaller once Ta doping exceeds the critical concentration. The Bode phase plots shown in Fig. 4 can prove the faster electron transportation in the doped electrode with the slight left-shift of the characteristic frequency, implying a longer electron lifetime in the doped electrode. The lifetime of electrons in the oxide film (τ_r) can be estimated from the maximum angular frequency (ω_{max}) of the impedance semicircle arc at middle frequencies, according to the relation $\tau_r=1/\omega_{max}=1/2\pi f_{max}$, where f_{max} is the maximum frequency of the mid-frequency peak.[2, 31] From the Bode-phase plots shown in Fig. 4, the f_{max} values for 0.3% Ta doped- and pristine TiO_2 device are estimated to be 5.7 and 7.5Hz, respectively. The small f_{max} value for doped device implies that a longer electron lifetime could be expected, which means that the produced electrons can diffuse further without interruption, such as recombination and trapping within the film. These factors are directly related to the improved efficiency of these DSSCs.

Conclusions

A flame spray pyrolysis approach was employed to dope tantalum ions homogeneously into TiO_2 nanoparticles and the mechanism of tantalum doping on the V_{oc} variability for DSSCs was studied. The enhanced electron concentration derived from Ta^{5+} doping is responsible for the open-circuit voltage improvement due to the upward shift of the Fermi level, but the oxygen defects generated retarded the negative shift of Fermi

level. By mediating the trap states in the host, highly efficient DSSC devices could be achieved with higher V_{oc}. The fast doping method may be extended to other metal cations, suggesting potential applications in photoelectric conversion and catalysis.

Acknowledgements

We acknowledge the funding support from the National Natural Science Foundation of China (20925621, 21136006, 21176068) and Singapore National Research Foundation (CREATE Programme of Nanomaterials for Energy and Water Management).

Notes and references

[a] *Key Laboratory for Ultrafine Materials of Ministry of Education, East China University of Science and Technology, Shanghai 200237, China. Email: gufeng@ecust.edu.cn, huyanjie@ecust.edu.cn.*
[b] *School of Materials Science and Engineering, Nanyang Technological University, Singapore 639798, Singapore.*

† Electronic Supplementary Information (ESI) available: Detailed experimental section, DSSC device assembly and characterization, XRD patterns, additional SEM, TEM pictures, XPS resluts and photographs of powders heat-treated in different atmosphere. See DOI: 10.1039/b000000x/

1. M. Gratzel, *Nature*, 2001, 414, 338-344.
2. J. F. Qian, P. Liu, Y. Xiao, Y. Jiang, Y. L. Cao, X. P. Ai and H. X. Yang, *Adv. Mater.*, 2009, 21, 3663-3667.
3. N. Memarian, I. Concina, A. Braga, S. M. Rozati, A. Vomiero and G. Sberveglieri, *Angew. Chem. Int. Ed.*, 2011, 50, 12321-12325.
4. X. J. Feng, K. Zhu, A. J. Frank, C. A. Grimes and T. E. Mallouk, *Angew. Chem. Int. Ed.*, 2012, 51, 2727-2730.
5. A. Yella, H. W. Lee, H. N. Tsao, C. Y. Yi, A. K. Chandiran, M. K. Nazeeruddin, E. W. G. Diau, C. Y. Yeh, S. M. Zakeeruddin and M. Gratzel, *Science*, 2011, 334, 629-634.
6. X. J. Feng, K. Shankar, M. Paulose and C. A. Grimes, *Angew. Chem. Int. Ed.*, 2009, 48, 8095-8098.
7. A. Hagfeldt, G. Boschloo, L. C. Sun, L. Kloo and H. Pettersson, *Chem. Rev.*, 2010, 110, 6595-6663.
8. F. Zhu, P. P. Zhang, X. J. Wu, L. M. Fu, J. P. Zhang and D. S. Xu, *ChemPhysChem*, 2012, 13, 3731-3737.
9. E. Palomares, J. N. Clifford, S. A. Haque, T. Lutz and J. R. Durrant, *J. Am. Chem. Soc.*, 2003, 125, 475-482.
10. A. Kay and M. Gratzel, *Chem. Mater.*, 2002, 14, 2930-2935.
11. K. G. Stamplecoskie, L. Ju, S. S. Farvid and P. V. Radovanovic, *Nano Lett.*, 2008, 8, 2674-2681.
12. D. E. Perea, E. R. Hemesath, E. J. Schwalbach, J. L. Lensch-Falk, P. W. Voorhees and L. J. Lauhon, *Nat. Nanotechnol.*, 2009, 4, 315-319.
13. X. J. Lu, X. L. Mou, J. J. Wu, D. W. Zhang, L. L. Zhang, F. Q. Huang, F. F. Xu and S. M. Huang, *Adv. Funct. Mater.*, 2010, 20, 509-515.
14. X. Zhang, F. Liu, Q. L. Huang, G. Zhou and Z. S. Wang, *J. Phys. Chem. C*, 2011, 115, 12665-12671.
15. M. Durr, S. Rosselli, A. Yasuda and G. Nelles, *J. Phys. Chem. B*, 2006, 110, 21899-21902.
16. K. H. Ko, Y. C. Lee and Y. J. Jung, *J. Colloid Interface Sci.*, 2005, 283, 482-487.
17. H. J. Snaith and L. Schmidt-Mende, *Adv. Mater.*, 2007, 19, 3187-3200.
18. J. Orenstein and M. Kastner, *Phys. Rev. Lett.*, 1981, 46, 1421-1424.
19. K. Lee and P. Schmuki, *Electrochem. Commun.*, 2012, 25, 11-14.
20. J. H. Choi, S. H. Kwon, Y. K. Jeong, I. Kim and K. H. Kim, *J. Electrochem. Soc.*, 2011, 158, B749-B753.
21. X. D. Feng, D. C. Sayle, Z. L. Wang, M. S. Paras, B. Santora, A. C. Sutorik, T. X. T. Sayle, Y. Yang, Y. Ding, X. D. Wang and Y. S. Her, *Science*, 2006, 312, 1504-1508.
22. R. Strobel and S. E. Pratsinis, *J. Mater. Chem.*, 2007, 17, 4743-4756.
23. J. Arbiol, J. Cerda, G. Dezanneau, A. Cirera, F. Peiro, A. Cornet and J. R. Morante, *J. Appl. Phys.*, 2002, 92, 853-861.
24. D. O. Scanlon, C. W. Dunnill, J. Buckeridge, S. A. Shevlin, A. J. Logsdail, S. M. Woodley, C. R. A. Catlow, M. J. Powell, R. G. Palgrave, I. P. Parkin, G. W. Watson, T. W. Keal, P. Sherwood, A. Walsh and A. A. Sokol, *Nat. Mater.*, 2013, 12, 798-801.
25. T. L. Ma, M. Akiyama, E. Abe and I. Imai, *Nano Lett.*, 2005, 5, 2543-2547.
26. N. Bonini, M. C. Carotta, A. Chiorino, V. Guidi, C. Malagu, G. Martinelli, L. Paglialonga and M. Sacerdoti, *Sens. Actuators, B*, 2000, 68, 274-280.
27. K.-Y. Yang, K.-Z. Fung and M.-C. Wang, *J. Appl. Phys.*, 2006, 100, 056102.
28. P. Claus, A. Bruckner, C. Mohr and H. Hofmeister, *J. Am. Chem. Soc.*, 2000, 122, 11430-11439.
29. V. E. Henrich, G. Dresselhaus and H. J. Zeiger, *Phys. Rev. Lett.*, 1976, 36, 1335-1339.
30. P. R. F. Barnes, K. Miettunen, X. E. Li, A. Y. Anderson, T. Bessho, M. Gratzel and B. C. O'Regan, *Adv. Mater.*, 2013, 25, 1881-1922.
31. R. Kern, R. Sastrawan, J. Ferber, R. Stangl and J. Luther, *Electrochim. Acta*, 2002, 47, 4213-4225.

